
Chain of Thought in Order: Discovering Learning-Friendly Orders for Arithmetic

Yuta Sato¹ Kazuhiko Kawamoto¹ Hiroshi Kera^{1,2}

Abstract

The chain of thought, i.e., step-by-step reasoning, is one of the fundamental mechanisms of Transformers. While the design of intermediate reasoning steps has been extensively studied and shown to critically influence performance on mathematical, multi-step reasoning tasks, the ordering of these steps has received little attention, despite its significant effect on the difficulty of reasoning. This study addresses a novel task of unraveling the chain of thought—reordering decoder input tokens into a learning-friendly sequence for Transformers, for learning arithmetic tasks. The proposed pipeline first trains a Transformer on a mixture of target sequences arranged in different orders and then identifies benign orders as those with fast loss drops in the early stage. As the search space grows factorially in sequence length, we propose a two-stage hierarchical approach for inter- and intra-block reordering. Experiments on seven order-sensitive arithmetic tasks show that our method identifies a learning-friendly order out of a few billion candidates. Notably, it recovered the reverse-digit order reported in prior studies for the multiplication task.

1. Introduction

Autoregressive generation is central to the success of the Transformer (Vaswani et al., 2017) in reasoning tasks, such as end-to-end learning of arithmetic and symbolic computation tasks (Alfarano et al., 2024; Charton, 2022; Kera et al., 2024; 2025; Lample & Charton, 2020; Li et al., 2023a;b; Wenger et al., 2022). The autoregressive nature makes each reasoning step conditioned on the preceding context, and careful design of intermediate reasoning steps, known as *chain of thought*, guides the model’s reasoning toward the final answer of the target problem. For example, it has been known that learning the parity function—the prediction of

the parity of the input bit string—is challenging (Hahn & Rofin, 2024; Shalev-Shwartz et al., 2017). However, Kim & Suzuki (2025) has recently shown that the step-by-step prediction of the parity of the first k bits for $k = 1, 2, \dots$, makes learning successful.

One important yet underexplored aspect is the order of the chain of thought—not only which steps to include, but also how they are arranged can greatly impact learning. For example, Shen et al. (2023) has shown that Transformers learn multiplication of two integers with better generalization to larger integers (i.e., those with more digits) when the product is predicted from least to most significant digits (cf. Figure 1). While this particular case can be explained by the carries, which flow from least to most significant digits, a systematic way of determining a learning-friendly order of the chain of thought¹ remains unknown.

In this study, we address a new task of reordering decoder input tokens into a learning-friendly order for better learning of arithmetic tasks. Exploiting the observation that neural networks tend to learn from easy to hard instances during training (Arpit et al., 2017; Forouzesh & Thiran, 2024; Swayamdipta et al., 2020), we train a lightweight Transformer on a mixture of target sequences in different orders and identify those that lead to a faster loss drop in the early stages of training. To better handle longer sequences, we propose a two-stage hierarchical approach, where the global stage finds block-level orders, while the local stage refines the order within each block.

The experiments demonstrate that the proposed method turns training successful by reordering target sequences. We designed six arithmetic tasks that are relatively easy to compute with the (input and) target sequence in the forward order, but not with other orders. The proposed method succeeds in discovering the optimal order for sequences of length up to 13 (i.e., roughly 10^9 permutations) with randomized initial candidates, and structured candidates extend it to length 40 (i.e., roughly 10^{47} permutations), increasing the success rate of arithmetic computation from approxi-

¹Chiba University ²National Institute of Informatics. Correspondence to: Hiroshi Kera <kera@chiba-u.jp>.

¹Chain of thought is well-known as prompting techniques (e.g., Wei et al. (2022)), but it also covers direct training or fine-tuning to generate reasoning steps (e.g., Kim & Suzuki (2025)). Our setup follows the latter. See (Chu et al., 2024) for a survey.

mately 10% to 100%. We also applied our method to the multiplication task in Shen et al. (2023) and successfully rediscovered the reverse orders.

Our contributions are summarized as follows:

- We address a novel task of discovering a learning-friendly order of decoder input tokens. We define order-sensitive tasks and introduce six arithmetic instances that serve as a benchmark for this new task.
- We propose a two-stage exploration method that efficiently determines learning-friendly orders. The exploration maintains a set of candidate permutations, and the candidates are ranked and replaced based on the loss profiling, which exploits the nature of easy-to-hard learning of neural networks.
- The experiments demonstrate that our method scales to sequence lengths up to $L = 13$ with random initial candidates and $L = 40$ with structured initial candidates. In particular, our method rediscovered the observation reported in (Shen et al., 2023): the reverse order is learning-friendly for the integer multiplication task.

2. Related work

Transformers for mathematical tasks. Transformers have recently been applied to mathematical problem-solving with encouraging results. Lample & Charton (2020) has demonstrated that a Transformer can carry out integral calculus with a high success rate, suggesting sequence-to-sequence models can handle algebraic tasks. Since that study, applications have expanded to arithmetic (Charton, 2022), linear algebra (Charton, 2022), computational algebra (Kera et al., 2024; 2025), and coding theory, as well as cryptography (Li et al., 2023a;b; Wenger et al., 2022). One reason behind these successes is the autoregressive generation scheme. Although theory has suggested that learning high-sensitive functions such as parity is difficult (Hahn & Rofin, 2024), recent work achieved a high success rate on parity tasks by applying a chain of thought prompting (Chen et al., 2023; Kojima et al., 2022; Wei et al., 2022; Yao et al., 2023; Zhang et al., 2024) to arithmetic and by exploiting the generated output tokens effectively (Kim & Suzuki, 2025). Positional encoding is also crucial for arithmetic problems; prior work Jelassi et al. (2023) has shown that relative-position and abacus-style embeddings improve generalization to out-of-distribution data. These studies collectively show that task-specific representations and positional encodings strongly influence performance. In particular, prior work (Shen et al., 2023) analyzed in detail how digit order affects multiplication success rate and demonstrated that generating digits from the least significant position upward raises the success rate; however, the ordering was chosen heuristically rather than by an automated procedure. Systematic optimization

of the output order itself in arithmetic tasks remains unaddressed. This study is the first to exploratively optimize the output-sequence permutation for each task, automatically discovering a learning-friendly target order.

Easy-to-hard learning dynamics in deep neural networks. The observation that deep neural networks can be trained even on randomly assigned labels—while still achieving excellent generalization on real data—led to a line of research into how models adapt to data during training (Zhang et al., 2017). Arpit et al. (2017) has experimentally shown that networks first pick up simple regularities between inputs and labels and only later transition to memorizing harder, noise-like examples. More broadly, deep neural networks are known to learn easy instances in a dataset before gradually fitting the more difficult ones; in image domains, this behavior is often referred to as spectral bias (Rahaman et al., 2019). This property is now widely exploited in curriculum learning (Baldock et al., 2021; Han et al., 2018; Jiang et al., 2018) and data-quality control (Swayamdipta et al., 2020). For example, integrating each sample’s learning curve can reveal mislabeled data (Forouzesh & Thiran, 2024). Most prior work, however, analyzes such dynamics by injecting noise directly into the target labels themselves. In contrast, this study focuses on the ordering of the target sequences. The dataset is rearranged with multiple permutation matrices, and the model is trained on these reordered versions to investigate how sequence order affects learning.

3. Unraveling the Chain of Thought

The Transformer decoder generates output sequences in an autoregressive manner. Autoregressive generation with a proper order strongly improves the reasoning ability of Transformers. For example, Figure 1 shows that, in the task of multiplying two integers, the digits of the target integer (each treated as a token) should be presented in reverse order—from lower to higher digits—because this lets the Transformer learn to compute carries step by step through autoregressive generation.

Order sensitivity. If the operation counts in autoregressive computation for a task have a non-trivial gap between two orders, approaching infinity as the sequence length grows, we refer to the task as order sensitive. A formal definition can be found in Section D. One can define an order-sensitive task using recurrence and an irreversible function.

Example 3.1 (ReLU sequence). Let $X = [x_1, \dots, x_L]$ be a sequence of integers. Let $y_1 = x_1$ and for $i = 2, \dots, L$,

$$y_i = \text{ReLU}(x_i + y_{i-1}) := \max(x_i + y_{i-1}, 0). \quad (1)$$

Then, autoregressive generation with the input sequence X and the target sequence in natural causal order, i.e.,

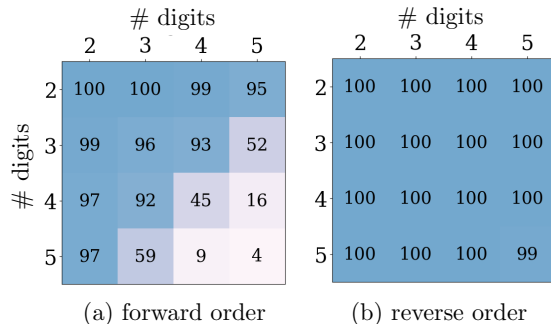


Figure 1. Success rates for the multiplication of two integers, reproducing (Shen et al., 2023). Matrix rows and columns indicate the number of digits in each operand. Evaluation is conducted with 100 samples for each digit position. (a) The model is trained to output from the most significant digit. (b) The model is trained to output from the least significant digit.

$Y = [y_1, \dots, y_L]$, determines the next token y_i locally by the immediate context (e.g., y_{i-1} and x_i). However, in anti-causal orders (e.g., the reverse order $[y_L, \dots, y_1]$), this locality is broken. The application of the ReLU function is irreversible when $x_i + y_{i-1} \leq 0$, and this ambiguity forces the model to implicitly resolve the entire causal chain from the input to determine the correct token, significantly increasing the reasoning burden compared to the forward order. More examples with other irreversible functions will be introduced in Section 5.1 and discussed in Section D.

Our problem is to discover a target sequence order of the Transformer decoder that improves the learning of a given order-sensitive task.

Learning-friendly order. More formally, let Σ be the set of all tokens. We denote the set of all finite token sequences by Σ^* and its restriction to length- L sequences by Σ^L . Let $\mathcal{T}_\theta : \Sigma^* \times \Sigma^L \rightarrow \Sigma^L$ be a Transformer with parameter θ . We assume that the target sequence length is fixed. Now, let $(X, Y) \sim \mathcal{D}$ be an input–target sequence pair (X, Y) with $|Y| = L$ from a joint distribution \mathcal{D} . Let S_L be the set of all permutations over $\{1, \dots, L\}$. The empirical risk minimizer θ_{ERM} with finite sample set $D = \{(X_i, Y_i)\}_{i=1}^m$ and permutation $\pi \in S_L$ is

$$\theta_{\text{ERM}}^\pi = \arg \min_{\theta} \frac{1}{m} \sum_{i=1}^m \ell(\mathcal{T}_\theta, X_i, \pi(Y_i)), \quad (2)$$

where ℓ denotes a loss function. Our goal is to discover a permutation π that minimizes the expected risk:

$$\pi^* = \arg \min_{\pi \in S_L} \mathbb{E}_{(X, Y) \sim \mathcal{D}} [\ell(\mathcal{T}_{\theta_{\text{ERM}}^\pi}, X, \pi(Y))]. \quad (3)$$

Note that we hypothesize that learning-friendly orders and those requiring less operation counts for an order-sensitive task coincide. We only verify this empirically and theoretical justification is an interesting future work.

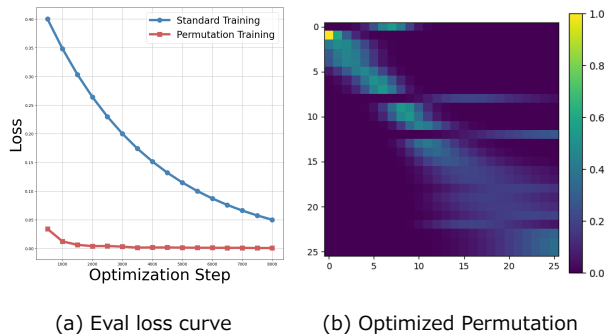


Figure 2. (a) Training-loss curves for a vanilla Transformer (blue) and for a model trained with soft-permutation optimization (red). (b) Permutation matrix learned during permutation training. Sparse off-diagonal weights clustered around the main diagonal indicate leakage from future tokens.

Optimizing soft permutation fails. A permutation $\pi(Y)$ of a target sequence $Y = [y_1, \dots, y_L] \in \Sigma^L$ can be represented as a matrix product YP , where $P \in \{0, 1\}^{L \times L}$ is a permutation matrix. The optimization over permutation matrices is challenging because one has to test all possible permutations, which is $L!$ for those over $\{1, \dots, L\}$. One may introduce a soft permutation matrix $\tilde{P} \in [0, 1]^{L \times L}$ and perform empirical risk minimization jointly over θ and \tilde{P} . However, such joint optimization leads to immediate failure because the soft permutation creates a shortcut to future tokens, undermining the objective of next-token prediction. Figure 2 shows such an approach leads to an immediate loss drop at the early stage of training, because the soft permutation \tilde{P} causes information leakage from future tokens; each token in $Y_i P$ is a soft mixture of all the tokens in Y , which undermines the next-token prediction. Introducing an additional loss that strongly penalizes non-dominant entries in \tilde{P} and encourages it to approximate a hard permutation matrix P can mitigate such leakage (see Section B.2). However, training over nearly hard permutation matrices induces a highly non-convex loss surface, and the optimization process is prone to getting trapped in local minima (Jang et al., 2017; Mena et al., 2018).

4. Proposed method

We propose a strategy to discover a suitable permutation of target token sequences. The key idea is to leverage a characteristic of the training dynamics of deep neural networks: they tend to learn easy samples in the early stages of training, and gradually adapt to harder samples later. This phenomenon has been reported in several contexts in the literature, such as Arpit et al. (2017) for learning with noisy labels and Baldock et al. (2021) for identifying difficult examples.

We discovered this is also the case with the training with different decoder token orders, see Figure 3. Exploiting this observation, we proposed to train a Transformer only for a few epochs on a dataset with various orders in mixture and identify learning-friendly orders as “easy samples,” for which the loss drops faster.

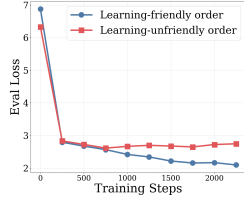


Figure 3. Evaluation loss curves when trained with two different orders.

More formally, let $D = \{(X_i, Y_i)\}_{i=1}^m$ and $D' = \{(X'_i, Y'_i)\}_{i=1}^{m'}$ be training and validation sets, respectively. Let $\mathcal{P} = \{P_1, \dots, P_T\}$ be the set of T candidate permutation matrices. Let D^{P_t} be the set D with reordered target sequences by P_t , i.e., $D^{P_t} = \{(X_i, Y_i P_t)\}_{i=1}^m$.

We determine learning-friendly orders through the following *loss profiling*.

- P1.** Let $E \in \mathbb{N}$. Train a Transformer for E epochs on a mixed dataset $\bar{D} := \bigcup_{t=1}^T D^{P_t}$. Let $\mathcal{T}_{\theta'}$ be the Transformer after training.
- P2.** Compute the loss on the validation set D' for each permutation; namely, for $t = 1, \dots, T$, compute

$$\mathcal{L}(D', P_t) = \frac{1}{m'} \sum_{i=1}^{m'} \ell(\mathcal{T}_{\theta'}, X'_i, Y'_i P_t). \quad (4)$$

Then, the most learning-friendly order $P^* := P_\tau$ is determined with $\tau = \arg \min_t \mathcal{L}(D', P_t)$.

Our experiments empirically observed that a few thousand permutations can be handled at once through this approach. However, the number of permutations grows factorially, which leads us to introduce the following two-stage hierarchical optimization, where aforementioned loss profiling (i.e., **P1** and **P2**) is performed to determine learning-friendly orders at each level.

Figure 4 illustrates our hierarchical method. We start with the initial set of permutation candidates $\mathcal{P}_0 = \{P_1, \dots, P_T\}$. The global stage splits each token sequence into several blocks and finds a good permutation at the block level. The local stage refines this coarse ordering by permuting the tokens within each block discovered at the global stage. Formally, the two stages operate as follows.

Global stage. Let the search depth be K and $T = 2K!$. Let $\mathcal{P}_1 := \mathcal{P}_0$. For $k = 1, \dots, K$, we conceptually split each target sequence into k blocks,² and apply the loss profiling to the new permutation set:

$$\bigcup_{P \in \mathcal{P}_k} \{PQ_1, \dots, PQ_{k!}\} \cup \{PQ_1 J, \dots, PQ_{k!} J\}, \quad (5)$$

²When $k = 1$, the sequence is not split into blocks

where $Q_i \in [0, 1]^{L \times L}$ are the block-level permutations and $J \in [0, 1]^{L \times L}$ is the exchange matrix (reversal permutation). The best $\lfloor T/2k! \rfloor$ permutations define the new candidate set \mathcal{P}_{k+1} , where $\lfloor \cdot \rfloor$ denotes the floor function. We denote the best permutation obtained in the final iteration ($k = K$) as P_g . This permutation is then refined with the local stage.

Local stage. Let $P_1 := P_g$ be the initial permutation. We again conceptually split each target sequence into blocks of size l . Let $R_1^i, \dots, R_{l_i}^i \in [0, 1]^{L \times L}$ be all the permutations inside the i -th block. These permutations do not change the orders outside the i -th block. For each block length $l \in \{2, 3, \dots, \lfloor L/2 \rfloor\}$ ³, we apply the loss profiling to the new candidate set:

$$\bigcup_{i=1}^{\lceil L/l \rceil} \{PR_1^i, \dots, PR_{l_i}^i\}, \quad (6)$$

and denote the lowest-loss result by P_l , where $\lceil \cdot \rceil$ is the ceiling function. Keeping each block’s internal order fixed, we perform loss profiling over the $\lfloor L/l \rfloor$ block-reordering candidates:

$$\{P_l Q'_1, P_l Q'_2, \dots, P_l Q'_{\lfloor L/l \rfloor}\}, \quad (7)$$

where $Q'_i \in [0, 1]^{L \times L}$ are the block-level permutations. The best candidate becomes the initial permutation for the next block size $l + 1$.

Computational overheads. While the proposed framework repeats training to narrow down the permutations to learning-friendly ones, several aspects keep it practically efficient. First, each of the training runs only for 800–1,600 steps (equivalently, 1–2 epochs with 10^5 samples of batch size 128) as the difference of loss drop speeds between candidate permutations becomes evident in the early stage. Second, a single training can handle around ten thousand permutations (up to $2 \times 7! = 10,080$ in our experiments). Third, our global–local framework provides efficient exploration. Specifically, with a global-stage depth of K , it needs K runs of training, and the local stage needs $2(\lfloor L/2 \rfloor - 1)$ runs. It is also worth noting that using a small Transformer model in the exploration is sufficient, as the learning-friendly orders should be independent of the model size.

5. Experiments

5.1. Order-sensitive arithmetic tasks

We evaluate our method on six order-sensitive arithmetic tasks. All tasks are designed so that the left-to-right (forward) order admits an incremental computation with a low computational complexity, while reversing the target order destroys the causal dependency most.

³When l does not divide L , the remaining $L \bmod l$ tokens are placed in an additional block.

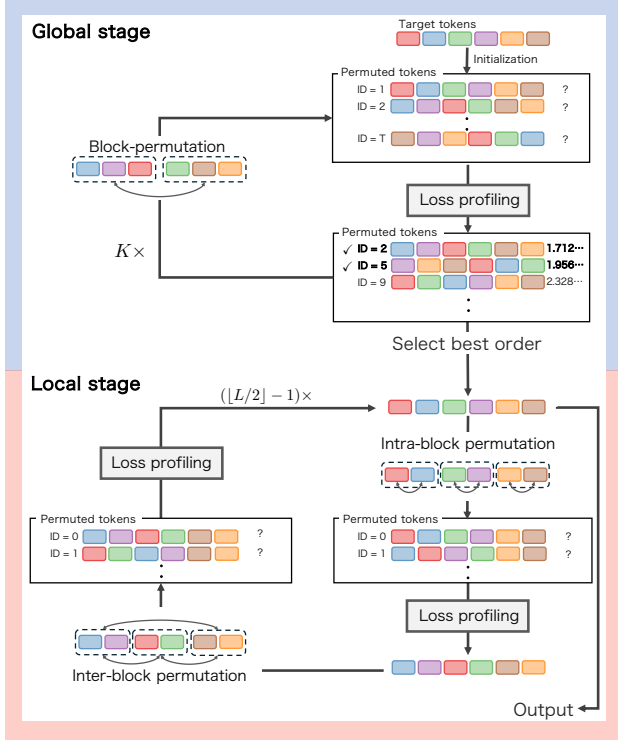


Figure 4. Search flow of our hierarchical approach. **Global stage:** The proposed method generates T candidate permutations by swapping the sequence at the macro-level, exchanging token blocks to quickly spot coarse, learning-friendly orders. **Local stage:** inside each chosen block, the proposed method further permutes the tokens, refining the sequence to discover a final permutation that maximizes learning ease.

RELU. The recurrence performs a rectified cumulative sum: $y_1 = x_1$ and for $i \geq 2$,

$$y_i = \text{ReLU}(x_i + y_{i-1}), \quad (8)$$

where $\text{ReLU}(z) = \max(z, 0)$ for $z \in \mathbb{R}$.

SQUARE. We output the squared-sum modulo a prime: $y_1 = x_1$ and for $i \geq 2$,

$$y_i = (x_i^2 + y_{i-1}^2) \bmod N. \quad (9)$$

where N is a fixed prime number.

MLP. We use an MLP inside the recurrence: $y_1 = x_1$ and for $i \geq 2$,

$$y_i = \lfloor \text{MLP}(x_i, y_{i-1}) \rfloor \bmod N, \quad (10)$$

where N is the vocabulary size. The MLP with h hidden units is defined as $\text{MLP}(u, v) = W_2 \text{ReLU}(W_1[u, v]^T + b_1) + b_2$, with $W_1 \in \mathbb{R}^{h \times 2}$, $b_1 \in \mathbb{R}^h$, $W_2 \in \mathbb{R}^{1 \times h}$, and $b_2 \in \mathbb{R}$ sampled once (e.g., He initialization; He et al. (2015)) and then fixed.

Table 1. Success rates over evaluation sets. For each task and length, a Transformer model was trained with a fixed target sequence (forward or reverse). The forward order is significantly more learning friendly. See Section 5.2 for the experiment setup.

| Task | Target Length | Success Rate (%) | |
|----------|---------------|------------------|---------|
| | | Forward | Reverse |
| RELU | $L = 20$ | 99.6 | 5.6 |
| | $L = 50$ | 99.9 | 0.6 |
| SQUARE | $L = 20$ | 100 | 0.1 |
| | $L = 50$ | 100 | 0.0 |
| TRIANGLE | $L = 20$ | 100 | 0.2 |
| | $L = 50$ | 100 | 0.0 |
| MLP | $L = 20$ | 100 | 9.4 |
| | $L = 50$ | 100 | 0.6 |
| SINE | $L = 20$ | 100 | 6.2 |
| | $L = 50$ | 100 | 0.3 |
| CUBIC | $L = 20$ | 100 | 1.6 |
| | $L = 50$ | 100 | 0.0 |

SINE. A periodic nonlinear map with quantization: $y_1 = x_1$ and for $i \geq 2$,

$$y_i = \left\lfloor A \sin\left(\frac{2\pi}{P}(y_{i-1} + x_i)\right) \right\rfloor \bmod N, \quad (11)$$

where (A, P, N) are fixed constants.

CUBIC. A cubic recurrence modulo a prime: $y_1 = x_1$ and for $i \geq 2$,

$$y_i = (y_{i-1}^3 + x_i) \bmod N, \quad (12)$$

where N is a fixed prime number.

TRIANGLE. A piecewise-linear triangle-wave recurrence: $y_1 = x_1$ and for $i \geq 2$,

$$y_i = \left| ((y_{i-1} + x_i) \bmod 2N) - N \right|, \quad (13)$$

where N is a fixed amplitude parameter.

Table 1 empirically shows that there is a large gap in success rates between forward and reverse orders on these tasks. Formal verification by the operation counts can be found in Definition D.1. We also provide dataset parameters (e.g., N) and input–output examples in Section E.1.

5.2. Experimental setup

We provide a basic experimental setup. Further details will be specified in the subsequent sections or in the appendix.

Datasets. We generated datasets for the six arithmetic tasks given in Section 5.1. We considered both fixed-length and variable-length cases. We used $L \in \{5, 6, \dots, 50\}$ for the former, and L from two ranges, $L \in \{20, 21, \dots, 30\}$ and $L \in \{40, 41, \dots, 50\}$, for the latter. We prepared training

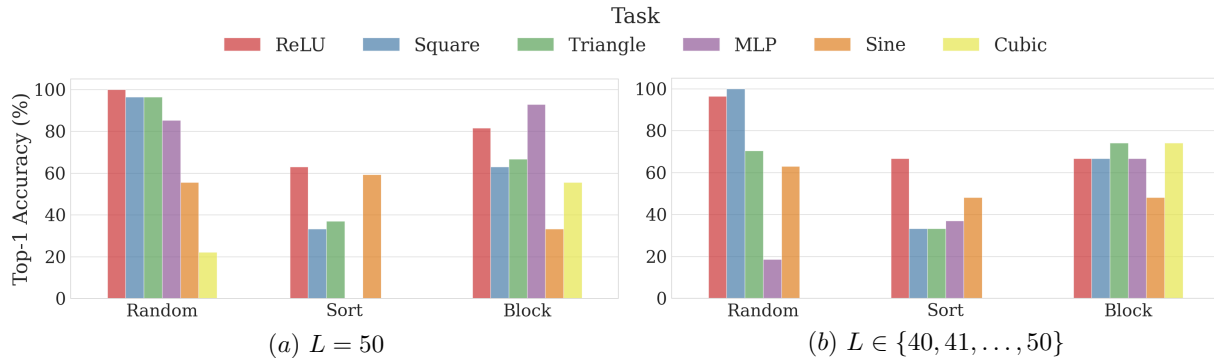


Figure 5. Top-1 identification accuracy of loss profiling: (a) fixed-length targets; (b) variable-length targets. Each run is initialized with one of the permutation sets Random \mathcal{P}_r , Sort \mathcal{P}_s , or Block \mathcal{P}_b .

(size 10^5), validation (size 10^3) for exploration, and evaluation (size 10^3) sets for final training, using random seeds 42, 84, and 123, respectively.

Exploration setup. The proposed global–local method explores learning-friendly orders. As described in Section 4, small, lightweight GPT-2 models (Radford et al., 2019) are repeatedly trained for a small number of steps, and the loss profiling ranks permutation candidates using the validation set. Training settings are detailed in Section E.2. The configuration of GPT-2 models and the initialization of the candidate permutations of global–local search will be specified in the next sections.

Final Training setup. The proposed global–local exploration returns a learning-friendly order. In the final training phase, a full training of a GPT-2 model is performed on the training set with target sequences in the discovered order, and the success rate over the evaluation set is measured. The success rate is defined as the proportion of evaluation samples where the Transformer outputs an entirely correct target sequence. The final training uses a larger GPT-2 model than those used in the exploration phase to pursue the final success rate. Particularly, it has six layers and eight attention heads with embedding and feed-forward dimensions $(d_{\text{emb}}, d_{\text{ffn}}) = (512, 2048)$.

5.3. Loss profiling for discovering the forward order

We first show that loss profiling successfully discovers the learning-friendly order from candidate sets. We consider three types of candidate sets. All three include the optimal (forward) order. Figure 10 provides the visualization.

- \mathcal{P}_r (**Random**) consists of the forward order and random orders (permutations). The forward order typically outperforms others by a large margin.
- \mathcal{P}_s (**Sort**) consists of partially sorted orders. The bubble sort algorithm (Knuth, 1998) reorders a random

permutation toward the forward order, and we evenly sample permutations from the sorting trajectory. This set ranges from learning-friendly (nearly sorted) orders to unfriendly (fully random) ones.

- \mathcal{P}_b (**Block**) consists of orders that are randomly shuffled at the block level. We fix the block size to $b = 5$. The last block can be smaller than b if b does not divide the sequence length. This candidates set is reasonable when one can assume good prior on the local structure.

Setup. To show the robustness of loss profiling up to the choice of model configurations, we tested 27 GPT-2 configurations by varying the number of layers $n_{\text{layer}} \in \{1, 2, 4\}$, attention heads $n_{\text{head}} \in \{1, 2, 4\}$, and model dimensions $(d_{\text{emb}}, d_{\text{ffn}}) \in \{(128, 512), (256, 1024), (512, 2048)\}$. Given a set of permutations \mathcal{P} , loss profiling assigns a score to each permutation. The permutations are ranked accordingly, and the top- k accuracy measures whether the forward order appears among the top k with particular emphasis on the top-1 case.

Top-1 accuracy. Figure 5(a) shows the top-1 accuracy in the fixed-length setting. Among the initialization sets, \mathcal{P}_r achieves the highest accuracy, successfully identifying the ground truth in nearly 90% of cases across RELU, SQUARE, TRIANGLE, and MLP tasks, regardless of model size. In contrast, \mathcal{P}_b and \mathcal{P}_s show relatively lower performance. This performance gap likely stems from the distinct characteristics of the permutation sets: \mathcal{P}_b and \mathcal{P}_s contain many candidates structurally similar to the forward order. These near-optimal permutations often yield comparable loss decreases to the forward order, making it challenging for loss profiling to single it out as the best one. Figure 5(b) shows the results in the variable-length case. The top-1 accuracy is comparable to the fixed-length case, indicating that loss profiling with simple padding works.

Model ablation. Figure 6 presents the impact of model dimensions on identification accuracy. For \mathcal{P}_r and \mathcal{P}_s , smaller

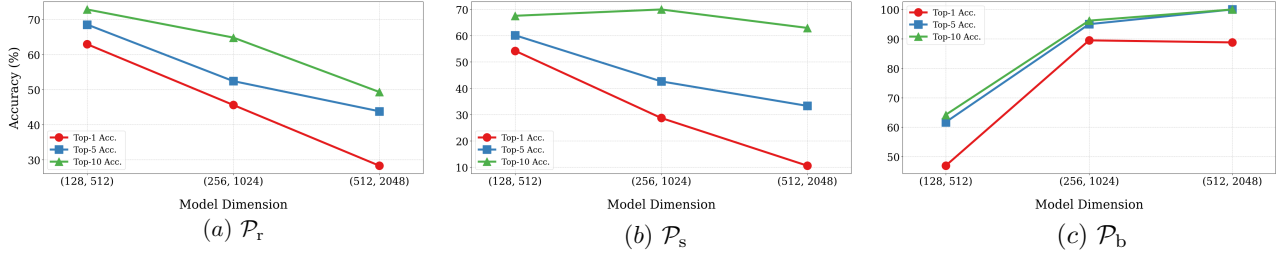


Figure 6. Identification accuracy of the forward order across various model dimensions, defined by pairs of $(d_{\text{emb}}, d_{\text{ffn}})$. Subplots (a), (b), and (c) show the results for the initialization sets \mathcal{P}_r , \mathcal{P}_s , and \mathcal{P}_b , respectively.

model dimensions yield higher identification accuracy. This implies that models with limited expressivity are more sensitive to the difficulty of the order, allowing them to adapt more easily to learning-friendly sequences, thereby justifying our use of lightweight models in the exploration stage. Conversely, for \mathcal{P}_b , higher model dimensions correlate with better identification accuracy. We hypothesize that when candidates are locally similar (as in block permutations), a larger model capacity is required to distinguish global structural differences.

5.4. Global-local exploration of learning-friendly orders

We now demonstrate that the proposed method can discover learning-friendly orders.

Setup. The basic setup follows the previous sections. We execute the global-local exploration with search depth K . We set $K = 6$ for short sequences ($10 \leq L \leq 13$) and $K = 7$ for longer ones ($20 \leq L \leq 40$) for better convergence. The exploration starts with either of the following initial candidate sets: $\mathcal{P}_r^-, \mathcal{P}_s^-, \mathcal{P}_b^-$. The superscript ‘-’ indicates that the forward order is replaced by a random permutation for \mathcal{P}_r and a block-level random one for \mathcal{P}_b . For \mathcal{P}_s^- , a random permutation is sorted toward the *reverse* order. For $L \geq 20$, only the global stage is conducted as the local stage is too costly. We tested four parameter combinations ($n_{\text{layer}} \in \{1, 2\}, n_{\text{head}} \in \{1, 2\}$) and present the results from the one with the highest success rate after final training. Given the analysis in Figure 6, we set $(d_{\text{emb}}, d_{\text{ffn}})$ to $(128, 512)$ for \mathcal{P}_r and \mathcal{P}_s , and to $(512, 2048)$ for \mathcal{P}_b .

Results on RELU, SQUARE, and TRIANGLE tasks. As shown in Table 3, the proposed method with \mathcal{P}_r^- is successful up to $L = 13$ for RELU and $L = 10$ for SQUARE and TRIANGLE. It is worth noting that the success in $L = 13$ and $L = 10$ implies singling out the forward order out of approximately $13! \approx 6 \times 10^9$ and $10! \approx 3 \times 10^6$ possibilities, respectively. The structured initialization \mathcal{P}_s^- and \mathcal{P}_b^- extend this to larger L . Given that the permutation space grows as $L!$, the length extension by 10 is significant. Particularly, \mathcal{P}_b^- is the most powerful initialization. This indicates the strong utility of leveraging prior knowledge on local

token ordering.

Results on MLP, SINE, and CUBIC tasks. Table 3 shows that MLP, SINE, and CUBIC are harder tasks. The structured initialization \mathcal{P}_s^- and \mathcal{P}_b^- still prove significant gain in MLP, SINE. The CUBIC task appears to be the hardest. This is because the cubic operations with modulo N encode a large integer space into $\{0, \dots, N - 1\}$, making the mapping complicated, making the learning hard even with the optimal order. Overall, Table 3 shows not only the success of the proposed method but also shows that the proposed tasks have diversity in the task level, and MLP, SINE, and CUBIC can serve as a good benchmark for future methods.

Runtime. Table 2 shows the overall runtime of the our method for the RELU task, measured on a single GPU of the NVIDIA A6000ada. The runtime is almost identical for other tasks as the training setup (e.g., training steps, input length) is identical. For harder tasks, the cost of the exploration phase becomes less dominant (cf. Table 5).

Table 2. Runtime breakdown of the exploration and final training phases for the RELU task.

| Params | Exploration [min] | | Final Training [min] |
|-----------------|-------------------|-------|----------------------|
| | Global | Local | |
| $K = 6, L = 10$ | 65.2 | 8.5 | 14.3 |
| $K = 6, L = 13$ | 68.5 | 12.8 | 15.0 |
| $K = 7, L = 20$ | 486.9 | — | 16.6 |
| $K = 7, L = 30$ | 563.5 | — | 20.1 |
| $K = 7, L = 40$ | 622.5 | — | 22.8 |

5.5. Rediscovering the optimal order for the PROD task

Shen et al. (2023) reported that least-significant-digit-first order (i.e., reverse order) is useful for learning integer-multiplication. Our method can rediscover this.

PROD. Let L be even. The input sequence is a concatenation of two left-zero-padded digits, i.e., $X = [a_1, \dots, a_{L/2}, b_1, \dots, b_{L/2}]$, where a_k, b_k are the k -th significant digits of integers a and b , respectively. The target sequence $[c_1, \dots, c_L]$ is the left-zero-padded sequence of digits of ab . As Figure 1 shows, the reverse order is known

Table 3. Success rates of final training using the permutations discovered by the global-local pipeline on the synthetic tasks. **Bold** indicates that the optimal (forward) order is successfully discovered.

| Initialization | Target Length | Task | | | | | |
|------------------------|---------------|-------------|--------------|--------------|--------------|--------------|--------------|
| | | RELU | SQUARE | TRIANGLE | MLP | SINE | CUBIC |
| \mathcal{P}_r^- | $L = 10$ | 99.6 | 100.0 | 100.0 | 38.2 | 54.2 | 0.3 |
| | $L = 13$ | 99.2 | 5.6 | 7.4 | 10.8 | 26.3 | 0.2 |
| | $L = 20$ | 24.2 | 10.4 | 0.8 | 5.9 | 8.2 | 0.0 |
| \mathcal{P}_s^- | $L = 20$ | 99.6 | 100.0 | 100.0 | 89.4 | 100.0 | 1.9 |
| | $L = 30$ | 97.6 | 100.0 | 100.0 | 100.0 | 100.0 | 3.8 |
| | $L = 40$ | 3.4 | 0.0 | 0.0 | 0.4 | 1.2 | 0.0 |
| \mathcal{P}_b^- | $L = 20$ | 99.6 | 100.0 | 100.0 | 100.0 | 100.0 | 100.0 |
| | $L = 30$ | 97.6 | 100.0 | 100.0 | 100.0 | 1.7 | 0.7 |
| | $L = 40$ | 96.0 | 2.1 | 1.2 | 100.0 | 0.0 | 0.0 |
| Reference Order | | | | | | | |
| Reverse | $L = 10$ | 2.7 | 6.5 | 3.5 | 10.4 | 21.8 | 0.6 |
| | $L = 13$ | 1.9 | 3.2 | 3.7 | 8.2 | 15.2 | 1.4 |
| | $L = 20$ | 5.6 | 0.1 | 0.2 | 9.4 | 6.2 | 1.6 |
| | $L = 30$ | 1.1 | 0.1 | 0.2 | 3.8 | 1.1 | 0.0 |
| | $L = 40$ | 0.9 | 0.0 | 0.0 | 0.8 | 0.7 | 0.0 |

Table 4. Success rates of final training on the PROD task using permutations discovered by the global-local pipeline. **Bold** indicates that the optimal (reverse) order is successfully discovered.

| Initialization | Target Length | Success Rate (%) | |
|-------------------|---------------|------------------|---------|
| | | Discovered | Forward |
| \mathcal{P}_r^- | $L = 10$ | 100.0 | 72.9 |
| | $L = 12$ | 51.4 | 51.4 |
| \mathcal{P}_s | $L = 20$ | 98.2 | 9.7 |
| \mathcal{P}_b^- | $L = 20$ | 98.2 | 9.7 |

Table 5. Runtime breakdown of the exploration and final training phases for the PROD task.

| Params | Exploration [min] | | Final Training [min] |
|-----------------|-------------------|-------|----------------------|
| | Global | Local | |
| $K = 6, L = 10$ | 116.7 | 78.8 | 470.2 |
| $K = 6, L = 12$ | 121.7 | 102.2 | 511.6 |
| $K = 7, L = 20$ | 599.7 | — | 639.5 |

to be learning friendly, while the forward order is not.

Setup. The general setup follows the previous experiments. Multiplication involves complex carry propagation, making it challenging to learn even in the optimal order. To address this, we scaled up the model size for the final training to a GPT-2 model with $n_{\text{layer}} = 12$, $n_{\text{head}} = 12$, and $(d_{\text{emb}}, d_{\text{fn}}) = (768, 3072)$. This configuration follows (Shen et al., 2023). The training set is also increased to 10^6 . In the training set, the numbers of digits of a, b were uniformly determined from $\{1, 2, \dots, L/2\}$ for each sample. In the evaluation set, the numbers of digits were uniformly sampled from $\{L/2 - 2, L/2 - 1, L/2\}$ as the hard samples concentrate on this part, as shown in Figure 1.

Results. Table 4 shows that our method successfully rediscovered the reverse order for \mathcal{P}_r^- with $L = 10$, and \mathcal{P}_s and \mathcal{P}_b^- with $L = 20$. The search fails for larger L because the learning itself becomes too difficult with the current model sizes, even with the optimal (reverse) order. Thus, the reverse order lacks immediate superiority over other orders, leading to limited success in loss profiling. Table 5 shows the runtime profile. As the PROD task requires a larger model and training set, the final training time was longer than in Table 2, and thus the exploration time is relatively less costly.

6. Conclusion

This study addressed a new task of reordering decoder input tokens for Transformers in learning arithmetic tasks. In essence, the proposed method performs short-term training on a mixture of target sequences in different orders and discovers easy samples for which the loss drops faster, as learning-friendly orders. To search the factorially large space efficiently, a two-stage hierarchical approach is adopted, combining global block-level exploration with local refinement. The experiments on six order-sensitive arithmetic tasks demonstrated that the proposed method discovers a learning-friendly order, improving the success rate from about 10% to near 100% and works for target lengths up to 13 tokens ($13! > 6 \times 10^9$ permutations). Moreover, the reverse-digit order reported in earlier work on the PROD task was rediscovered. Future work includes this to more general input sequences, such as natural languages.

Acknowledgments

This research was partially supported by JST PRESTO Grant Number JPMJPR24K, JST BOOST Program Grant Number JPMJBY24C6, and JSPS Program for Forming Japan’s Peak Research Universities (J-PEAKS) Grant Number JPJS00420230002, Mitsubishi Electric Information Technology R&D Center, and JSPS KAKENHI Grant Number JP23K24914.

References

- Alfarano, A., Charton, F., and Hayat, A. Global lyapunov functions: a long-standing open problem in mathematics, with symbolic transformers. In *Advances in Neural Information Processing Systems*, 2024.
- Arpit, D., Jastrzundefinedbski, S., Ballas, N., Krueger, D., Bengio, E., Kanwal, M. S., Maharaj, T., Fischer, A., Courville, A., Bengio, Y., and Lacoste-Julien, S. A closer look at memorization in deep networks. In *International Conference on Machine Learning*, 2017.
- Baldock, R. J. N., Maennel, H., and Neyshabur, B. Deep learning through the lens of example difficulty. In *Advances in Neural Information Processing Systems*, 2021.
- Charton, F. Linear algebra with transformers. *Transactions on Machine Learning Research*, 2022.
- Chen, W., Ma, X., Wang, X., and Cohen, W. W. Program of thoughts prompting: Disentangling computation from reasoning for numerical reasoning tasks. *Transactions on Machine Learning Research*, 2023.
- Chu, Z., Chen, J., Chen, Q., Yu, W., He, T., Wang, H., Peng, W., Liu, M., Qin, B., and Liu, T. Navigate through enigmatic labyrinth a survey of chain of thought reasoning: Advances, frontiers and future. In *Proceedings of the 62nd Annual Meeting of the Association for Computational Linguistics (Volume 1: Long Papers)*, pp. 1173–1203, 2024.
- Forouzesh, M. and Thiran, P. Differences between hard and noisy-labeled samples: An empirical study. In *Proceedings of the 2024 SIAM International Conference on Data Mining (SDM)*, pp. 91–99, 2024.
- Hahn, M. and Rofin, M. Why are sensitive functions hard for transformers? In *Proceedings of the Annual Meeting of the Association for Computational Linguistics*, 2024.
- Han, B., Yao, Q., Yu, X., Niu, G., Xu, M., Hu, W., Tsang, I., and Sugiyama, M. Co-teaching: Robust training of deep neural networks with extremely noisy labels. In *Advances in Neural Information Processing Systems*, 2018.
- He, K., Zhang, X., Ren, S., and Sun, J. Delving deep into rectifiers: Surpassing human-level performance on imagenet classification. In *Proceedings of the IEEE international conference on computer vision*, pp. 1026–1034, 2015.
- Jang, E., Gu, S., and Poole, B. Categorical reparameterization with gumbel-softmax. In *International Conference on Learning Representations*, 2017.
- Jelassi, S., d’Ascoli, S., Domingo-Enrich, C., Wu, Y., Li, Y., and Charton, F. Length generalization in arithmetic transformers, 2023.
- Jiang, L., Zhou, Z., Leung, T., Li, L.-J., and Fei-Fei, L. Mentornet: Learning data-driven curriculum for very deep neural networks on corrupted labels. In *International Conference on Machine Learning*, 2018.
- Kera, H., Ishihara, Y., Kambe, Y., Vaccon, T., and Yokoyama, K. Learning to compute gröbner bases. In *Advances in Neural Information Processing Systems*, 2024.
- Kera, H., Pelleriti, N., Ishihara, Y., Zimmer, M., and Pokutta, S. Computational algebra with attention: Transformer oracles for border basis algorithms. *arXiv:2505.23696*, 2025.
- Kim, J. and Suzuki, T. Transformers provably solve parity efficiently with chain of thought. In *International Conference on Learning Representations*, 2025.
- Knuth, D. E. *The Art of Computer Programming, Volume 3: Sorting and Searching*. Addison-Wesley Professional, 2nd edition, 1998.
- Kojima, T., Gu, S. S., Reid, M., Matsuo, Y., and Iwasawa, Y. Large language models are zero-shot reasoners. In *Advances in Neural Information Processing Systems*, 2022.
- Lample, G. and Charton, F. Deep learning for symbolic mathematics. In *International Conference on Learning Representations*, 2020.
- Li, C. Y., Sotáková, J., Wenger, E., Malhou, M., Garcelon, E., Charton, F., and Lauter, K. Salsapicante: A machine learning attack on lwe with binary secrets. In *Proceedings of the ACM SIGSAC Conference on Computer and Communications Security*, 2023a.
- Li, C. Y., Wenger, E., Allen-Zhu, Z., Charton, F., and Lauter, K. E. Salsa verde: a machine learning attack on learning with errors with sparse small secrets. In *Advances in Neural Information Processing Systems*, 2023b.
- Loshchilov, I. and Hutter, F. Decoupled weight decay regularization. In *International Conference on Learning Representations*, 2019.

- Mena, G., Belanger, D., Linderman, S., and Snoek, J. Learning latent permutations with gumbel-sinkhorn networks. In *International Conference on Learning Representations*, 2018.
- Radford, A., Wu, J., Child, R., Luan, D., Amodei, D., and Sutskever, I. Language models are unsupervised multitask learners. *OpenAI*, 2019.
- Rahaman, N., Baratin, A., Arpit, D., Draxler, F., Lin, M., Hamprecht, F., Bengio, Y., and Courville, A. On the spectral bias of neural networks. In *International Conference on Machine Learning*, 2019.
- Shalev-Shwartz, S., Shamir, O., and Shammah, S. Failures of gradient-based deep learning. In *International Conference on Machine Learning*, 2017.
- Shen, R., Bubeck, S., Eldan, R., Lee, Y. T., Li, Y., and Zhang, Y. Positional description matters for transformers arithmetic. *arXiv:2311.14737*, 2023.
- Swayamdipta, S., Schwartz, R., Lourie, N., Wang, Y., Hajishirzi, H., Smith, N. A., and Choi, Y. Dataset cartography: Mapping and diagnosing datasets with training dynamics. In *Proceedings of EMNLP*, 2020.
- Vaswani, A., Shazeer, N., Parmar, N., Uszkoreit, J., Jones, L., Gomez, A. N., Kaiser, L., and Polosukhin, I. Attention is all you need. In *Advances in Neural Information Processing Systems*, 2017.
- Wei, J., Wang, X., Schuurmans, D., Bosma, M., Ichter, B., Xia, F., Chi, E., Le, Q., and Zhou, D. Chain-of-thought prompting elicits reasoning in large language models. In *Advances in Neural Information Processing Systems*, 2022.
- Wenger, E., Chen, M., Charton, F., and Lauter, K. E. SALSA: attacking lattice cryptography with transformers. In *Advances in Neural Information Processing Systems*, 2022.
- Yao, S., Yu, D., Zhao, J., Shafran, I., Griffiths, T. L., Cao, Y., and Narasimhan, K. Tree of thoughts: Deliberate problem solving with large language models. In *Advances in Neural Information Processing Systems*, 2023.
- Zhang, C., Bengio, S., Hardt, M., Recht, B., and Vinyals, O. Understanding deep learning requires rethinking generalization. In *International Conference on Learning Representations*, 2017.
- Zhang, X., Du, C., Pang, T., Liu, Q., Gao, W., and Lin, M. Chain of preference optimization: Improving chain-of-thought reasoning in LLMs. In *Advances in Neural Information Processing Systems*, 2024.

A. Visualizing attention map

We present the attention maps obtained when training a Transformer on our proposed RELU task with datasets reordered in different ways. For this analysis, we use a GPT-2 model with a single layer and a single attention head. Figure 7 shows the attention maps for target length $L = 20$ under four target orders. The forward and reverse orders are defined in Section 5.1. The one-permuted order swaps exactly one pair of adjacent target tokens, whereas the random order is a random permutation of the forward sequence. Figure 8 illustrates how the attention maps change as the target length increases.

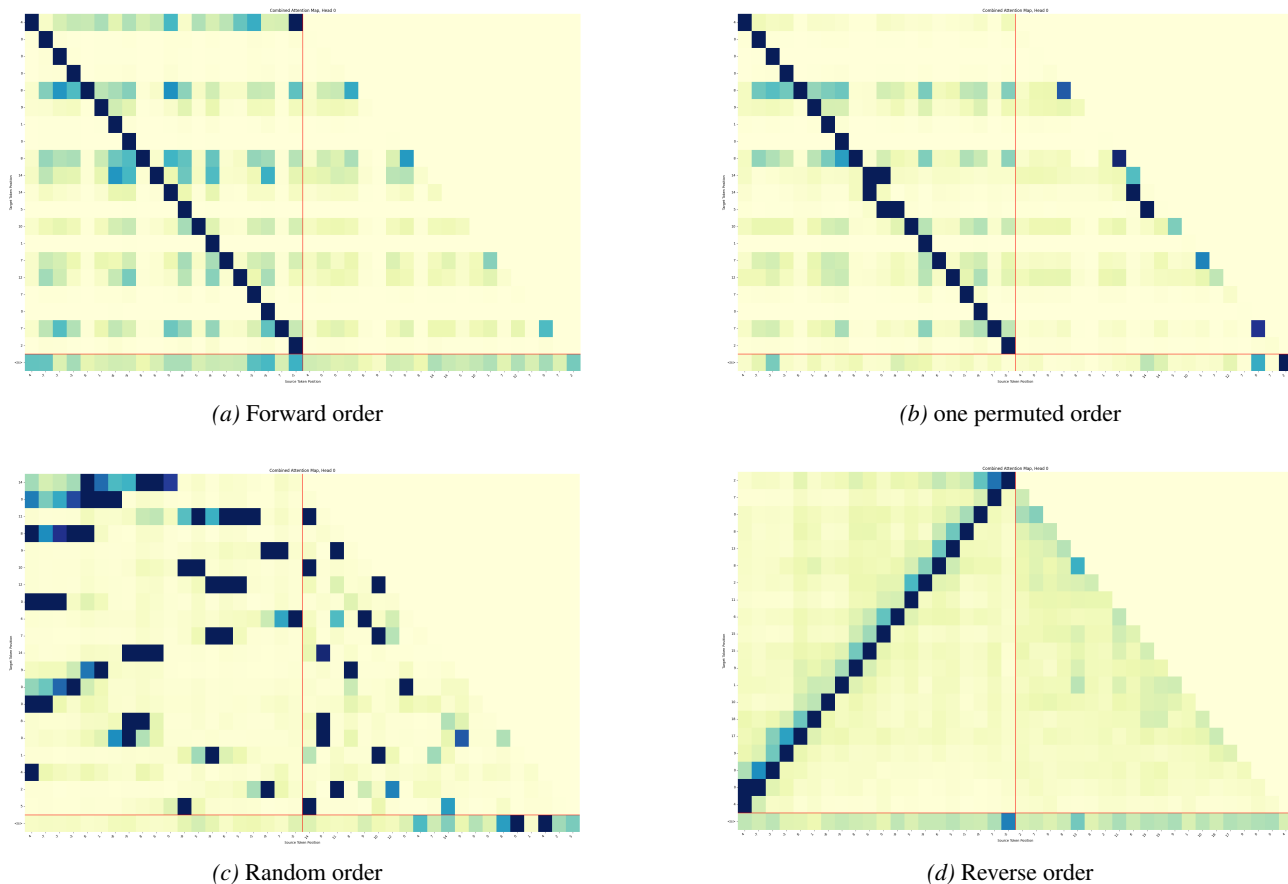


Figure 7. Attention matrices from models trained with four different target orders in the RELU task.

B. Soft-permutation optimization via attention sparsity

B.1. Analysis of information leakage in naive soft-permutation optimization

Before discussing the sparsity-based regularization, we address the fundamental limitation of optimizing a soft permutation matrix $\tilde{P} \in [0, 1]^{L \times L}$ jointly with the model parameters. We formulate the naive optimization objective as the minimization of the empirical risk:

$$\min_{\theta, \tilde{P}} \frac{1}{m} \sum_{i=1}^m \ell(\mathcal{T}_\theta, X_i, Y_i \tilde{P}). \quad (14)$$

However, as shown in Figure 2, such an approach leads to an immediate loss drop at the early stage of training. This creates a trivial solution where the soft permutation \tilde{P} causes information leakage from future tokens. Specifically, each token in the reordered target sequence $Y_i \tilde{P}$ becomes a soft mixture of all the tokens in the original sequence Y_i . In an auto-regressive setting, this mixture allows the model to access the ground truth of the next token (which is contained in the future positions of Y_i) through the non-zero off-diagonal entries of \tilde{P} , thereby undermining the next-token prediction task.

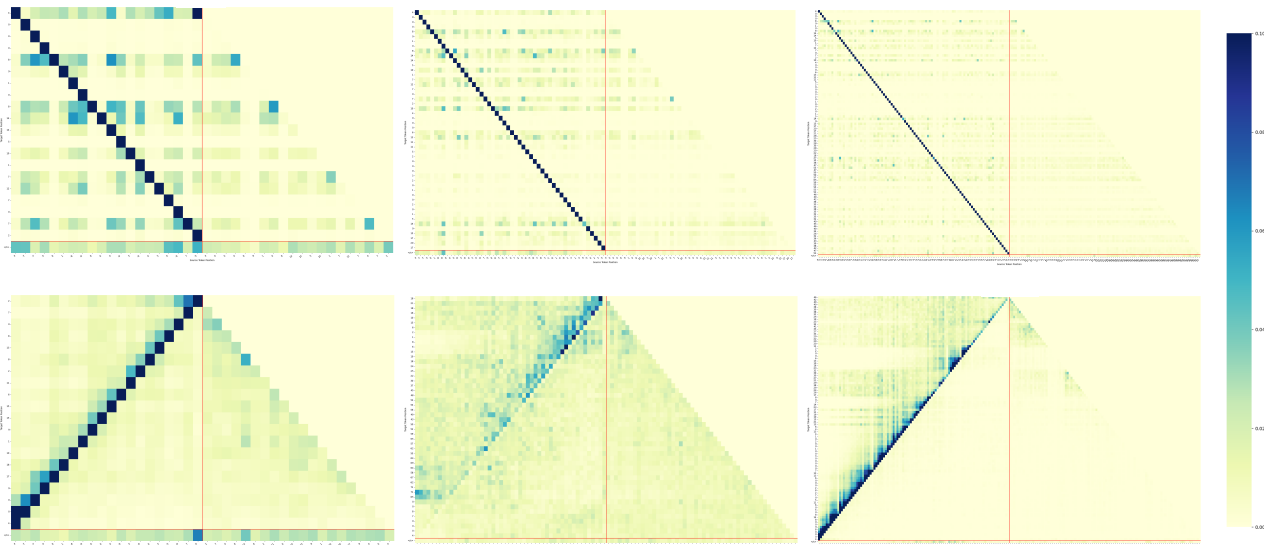


Figure 8. Differences in the attention matrices for the RELU task between forward and reverse orderings. The top three matrices correspond to models trained with forward order, and the bottom three with reverse order. Each pair of matrices shows results for input lengths $n = 20, 50,$ and $100,$ respectively.

Table 6. Attention sparsity S across target orders. A smaller value of S indicates greater sparsity.

| Task | Target length | Sparsity | |
|--------|-----------------|--------------|---------|
| | | Forward | Reverse |
| RELU | $L = 20$ | 1.160 | 1.640 |
| | $L = 50$ | 1.462 | 4.319 |
| | $L = 100$ | 1.687 | 3.195 |
| SQUARE | $L = 20$ | 1.117 | 1.531 |
| | $L = 50$ | 1.773 | 1.914 |
| | $L = 100$ | 1.407 | 1.990 |
| INDEX | $L = 13, d = 2$ | 0.848 | 2.574 |
| | $L = 13, d = 4$ | 0.887 | 1.486 |
| | $L = 13, d = 8$ | 1.116 | 1.596 |

Figure 2 (b) visualizes the learned soft permutation matrix obtained from this naive training. The matrix exhibits sparse off-diagonal weights clustered around the main diagonal. These weights indicate that the optimization process finds shortcuts to “peek” at the immediate future tokens rather than discovering a meaningful global causal ordering. This phenomenon motivates the need for alternative approaches, such as the attention sparsity regularization or the proposed discrete search pipeline, to prevent such leakage.

B.2. Analysis of attention sparsity.

To address the challenges of permutation optimization, we undertake a more detailed analysis of the attention mechanism. Intuitively, when the target order is learning-unfriendly, the local causal structure of the sequence is broken, meaning that more input and output tokens become relevant to predicting the next token. Conversely, for a learning-friendly order, we expect the attention map to be *sparser*, as the model can rely on specific local dependencies.

Let the query and key matrices be $Q, K \in \mathbb{R}^{L' \times d_{\text{emb}}}$, where L' is the decoder-input length and d_{emb} is the embedding

dimension. The self-attention weights are given by

$$A = \text{Softmax} \left(\frac{QK^\top}{\sqrt{d_{\text{emb}}}} \right) \in \mathbb{R}^{L' \times L'}, \quad (15)$$

where $\text{Softmax}(\cdot)$ is applied row-wise. Because each row of $A = (a_{ij})_{ij}$ is a probability vector, we define the mean sparsity S using the Shannon entropy:

$$S = -\frac{1}{L'} \sum_{i=1}^{L'} \sum_{j=1}^{L'} a_{ij} \log a_{ij}. \quad (16)$$

We compute S for models trained on both the forward (learning-friendly) and reverse (learning-unfriendly) orders of the order-sensitive tasks (Section 5.1). Table 6 shows that the forward order consistently yields lower S . Since a smaller S directly corresponds to lower entropy (i.e., higher sparsity), this confirms that learning-friendly orders produce sparser attention maps. Representative heat maps are provided in Section A.

Because S is derived solely from the learned attention weights, it is independent of the language-model loss and can serve as an orthogonal diagnostic metric. We explored optimizing permutations using an additional sparsity regularizer that explicitly rewards low-entropy attention. However, even with this bias, the optimizer failed to discover the learning-friendly order and instead converged to interleaved permutations, suggesting that sparsity guidance alone is insufficient to solve the permutation search in difficult regimes.

Specifically, we formulated a soft-permutation optimization method based on attention sparsity. In our two-stage strategy, we first optimize the Transformer parameters θ by minimizing the standard sequence-modeling loss over the training set:

$$\min_{\theta} \frac{1}{m} \sum_{i=1}^m \ell(\mathcal{T}_{\theta}, X_i, Y_i). \quad (17)$$

Next, denoting by $A(\tilde{P}) = [a_{ij}]$ the attention map produced when the target sequence is fed as $Y_i \tilde{P}$ into the Transformer, we optimize the soft permutation \tilde{P} by minimizing the total attention entropy:

$$\min_{\tilde{P}} S(A(\tilde{P})) = \min_{\tilde{P}} \left(-\frac{1}{L'} \sum_{i=1}^{L'} \sum_{j=1}^{L'} a_{ij} \log a_{ij} \right). \quad (18)$$

In our experiments, we alternated between these two optimization stages. Figure 9 compares the Stage 2 loss (entropy) under three conditions: the fixed learning-friendly order, the fixed learning-unfriendly (reverse) order, and the learned soft permutation. We observe that the soft permutation optimization does not significantly reduce the entropy-based loss relative to the fixed orders, nor does it converge to a genuinely structured ordering. This indicates that attention sparsity, while a useful diagnostic metric, is difficult to use as a direct reliable objective for permutation optimization due to optimization landscapes or trivial solutions.

C. Permutation search via evolutionary strategy

This section summarizes the evolutionary strategy (ES) baseline that we ran in parallel with our proposed method to search the permutation space. Each individual is a permutation P ; its fitness is the (negative) early-stage training loss of a Transformer trained with that order, so that permutations that are easier to learn receive higher scores. The ES is controlled by the population size N_p , crossover probability N_c , mutation probability N_m , number of generations N_g , tournament size N_t , and elitism ratio N_r , and proceeds as follows:

- (1) **Population initialization:** sample N_p random permutations.
- (2) **Selection:** pick parents via tournament selection with size N_t .
- (3) **Crossover:** with probability N_c , apply partially-mapped crossover to each selected pair.
- (4) **Mutation:** with probability N_m , swap two positions in the offspring permutation.

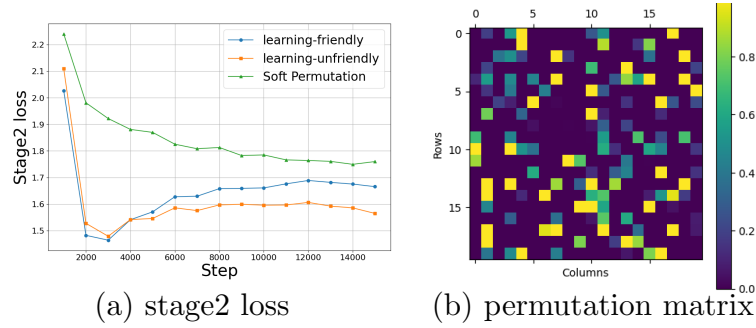


Figure 9. (a) Comparison of Stage 2 loss under fixed learning-friendly order, fixed learning-unfriendly order, and learned soft permutation. (b) shows a visualization of the learned soft permutation.

Table 7. Success rate obtained when the Transformer is retrained on the permutations discovered by the ES.

| Task | Input length | ES-discovered order | Success rate (%) | |
|--------|--------------|--|------------------|---------|
| | | | Retrain | Reverse |
| RELU | $L = 5$ | [2, 1, 0, 4, 3] | 26.9 | 10.4 |
| | $L = 10$ | [0, 1, 2, 3, 4, 5, 6, 7, 8, 9] | 100 | 3.5 |
| | $L = 20$ | [6, 7, 9, 8, 12, 11, 13, 18, 17, 14, 16, 15, 19, 5, 10, 1, 0, 3, 4, 2] | 9.2 | 0.7 |
| SQUARE | $L = 5$ | [1, 2, 3, 4, 0] | 100 | 21.5 |
| | $L = 10$ | [3, 4, 5, 6, 7, 8, 9, 1, 0, 2] | 99.9 | 6.5 |
| | $L = 20$ | [9, 10, 11, 12, 13, 14, 2, 3, 4, 5, 6, 15, 16, 17, 18, 19, 0, 1, 7, 8] | 5.2 | 0.1 |

(5) **Elitism:** evaluate every individual by

$$\text{fitness}(P) = -\frac{1}{m'} \sum_{i=1}^{m'} \ell(\mathcal{T}_\theta, X_i, Y_i P),$$

and copy the top N_r fraction to the next generation.

(6) **Termination:** stop when N_g generations have been processed.

Table 7 lists the permutation identified by the evolution strategy (ES) and the performance obtained when the model is retrained using that order.

D. Details on order-sensitive tasks

D.1. Order-sensitive tasks

Let Σ be the set of tokens. As defined in Section 3, we consider a task to be a deterministic mapping $F : \Sigma^* \rightarrow \Sigma^L$. For an input sequence $X \in \Sigma^*$, the target output is $Y = F(X) = [y_1, \dots, y_L] \in \Sigma^L$. We denote the set of all permutations over indices $\{1, \dots, L\}$ by S_L . For a fixed permutation $\pi \in S_L$, the reordered target sequence is denoted by $Y^{(\pi)} := [y_{\pi(1)}, \dots, y_{\pi(L)}]$.

To rigorously quantify the computational complexity of generating Y under a specific order, we first establish a cost model. Let Ω be a fixed set of primitive operators (e.g., $\{+, \times, \text{mod}, \text{ReLU}, \dots\}$), where each operator incurs a unit cost.

Stateless Sequential Generation. We define a sequential generation algorithm respecting order π as a tuple of stateless functions $A_\pi = (\phi_1, \dots, \phi_L)$. Each ϕ_t maps the available context to the next token $y_{\pi(t)}$. Crucially, to model the lack of recurrent state in standard Transformer inference (excluding the KV-cache of the outputs themselves), we impose a memoryless constraint: For every step $t \in \{1, \dots, L\}$, the function ϕ_t must compute the output $y_{\pi(t)}$ solely from the input

X and the previously generated partial sequence $Y_{<t}^{(\pi)} := [y_{\pi(1)}, \dots, y_{\pi(t-1)}]$:

$$y_{\pi(t)} = \phi_t \left(X, Y_{<t}^{(\pi)} \right). \quad (19)$$

Under this constraint, ϕ_t does not have access to any internal states, scratchpads, or intermediate computation results from preceding steps $\phi_1, \dots, \phi_{t-1}$.

The operation count of such an algorithm, denoted by $\text{Ops}(A_\pi; X)$, is the total number of operators from Ω invoked across all functions ϕ_1, \dots, ϕ_L . The minimal sequential cost is defined as:

$$C_\pi(X) := \min_{A_\pi} \text{Ops}(A_\pi; X), \quad (20)$$

where the minimization is over all algorithms A_π satisfying the memoryless constraint.

Order-Sensitivity. We characterize the difficulty of a task based on the disparity in computational cost between different generation orders.

Definition D.1 (Order sensitivity). Let \mathcal{D} be a distribution over inputs X . We define the *order-sensitivity ratio* $\rho(L)$ for a task F as the ratio of expected minimal costs between the worst-case order σ and the best-case order π :

$$\rho(L) := \sup_{\pi, \sigma \in \mathcal{S}_L} \frac{\mathbb{E}_{X \sim \mathcal{D}} [C_\sigma(X)]}{\mathbb{E}_{X \sim \mathcal{D}} [C_\pi(X)]}. \quad (21)$$

We classify the task F as **order-sensitive** if this ratio grows asymptotically with the sequence length L , i.e.,

$$\lim_{L \rightarrow \infty} \rho(L) = \infty. \quad (22)$$

D.2. Proof of order-sensitivity

We verify that the six tasks (RELU, SQUARE, MLP, SINE, CUBIC, TRIANGLE) proposed in Section 5 satisfy the definition of order-sensitivity. Specifically, we demonstrate that they are ρ -order-sensitive with $\rho(L) = \Theta(L)$.

Proposition D.2. The tasks RELU, SQUARE, MLP, SINE, CUBIC, and TRIANGLE are order-sensitive.

Proof. Let π_{fwd} be the forward order (identity permutation) and π_{rev} be the reverse order. We analyze the minimal sequential costs under the memoryless constraint defined in Section D.1.

Forward Complexity. In the forward order, the sequence is generated via a deterministic recurrence $y_1 = x_1$ and $y_i = f(x_i, y_{i-1})$ for $i = 2, \dots, L$. The optimal stateless algorithm simply executes this recurrence step-by-step. Since y_{i-1} is available in the immediate context $Y_{<i}^{(\pi_{\text{fwd}})}$, the cost to compute y_i is constant, denoted by c_f . Thus,

$$C_{\pi_{\text{fwd}}}(X) = \sum_{i=1}^L c_f = \Theta(L). \quad (23)$$

Reverse Complexity and Verification Cost. In the reverse order, the algorithm must generate y_L, y_{L-1}, \dots, y_1 . At step t (where the target is y_{L-t}), the available information is the input X and the suffix y_L, \dots, y_{L-t+1} . The algorithm must determine the preceding token y_{L-t-1} .

However, for all proposed tasks, the forward map $f(\cdot, y_{i-1})$ is non-injective with respect to y_{i-1} . Let $g_{x_i}(z) := f(x_i, z)$. The inverse map $g_{x_i}^{-1}(y_i)$ produces a set of candidates $\mathcal{S}_i = \{z \mid f(x_i, z) = y_i\}$ rather than a single value. For example, in SQUARE ($y_i = x_i^2 + y_{i-1}^2 \bmod N$), $|\mathcal{S}_i| \geq 2$ due to quadratic residues. Similarly, RELU and TRIANGLE map multiple inputs to the same output.

To identify the correct predecessor $y_{i-1}^* \in \mathcal{S}_i$ that is consistent with the initial condition $y_1 = x_1$, the algorithm must verify which candidate lies on the valid trajectory originating from x_1 . Under the **memoryless constraint**, the function ϕ_t cannot access internal states from previous steps. Therefore, the only way to deterministically verify a candidate is to re-compute the

forward trajectory from x_1 up to $i - 1$ and check if the result matches the candidate. This implies that generating the token at position i effectively incurs a cost of forward simulation from the start, which is proportional to i .

The minimal sequential cost for the reverse order is thus bounded by the sum of these verification costs:

$$C_{\pi_{\text{rev}}}(X) \approx \sum_{i=1}^L i = \frac{L(L+1)}{2} = \Theta(L^2). \quad (24)$$

Ratio. Combining the above, the order-sensitivity ratio is:

$$\frac{\mathbb{E}[C_{\pi_{\text{rev}}}(X)]}{\mathbb{E}[C_{\pi_{\text{fwd}}}(X)]} \approx \frac{\Theta(L^2)}{\Theta(L)} = \Theta(L). \quad (25)$$

This satisfies the condition $\lim_{L \rightarrow \infty} \rho(L) = \infty$, confirming the tasks are order-sensitive. \square

E. Details on experimental settings

In this section, we provide concrete examples of the datasets introduced in Section 5.2 and visualize the permutation sets used in our experiments.

E.1. Dataset examples

We present representative samples for the seven order-sensitive tasks described in Section 5.1. Table 8 summarizes the correspondence between the input X and the target Y , where Y represents the sequence in the forward (learning-friendly) order. Note that for the PROD task, the input consists of two integers a and b .

E.2. Experimental parameters and settings

We summarize the specific parameters used for the arithmetic tasks and the model training in Table 9 and Table 10, respectively.

In addition to the parameters listed in the tables, the following common configurations are applied across all experiments. Optimization is performed using AdamW (Loshchilov & Hutter, 2019) with $\beta_1 = 0.9$ and $\beta_2 = 0.999$. We employ a linearly decaying learning rate schedule starting from 5.0×10^{-5} . The dropout rate is set to 0.1, and positional embeddings are randomly initialized and optimized during training.

E.3. Permutation set visualization

Next, we visualize the three permutation sets ($\mathcal{P}_r, \mathcal{P}_s, \mathcal{P}_b$) introduced in Section 5.2. Figure 10 displays the sets used in the loss profiling experiments (Section 5.3), which include the forward order (Ground Truth) at ID=0. Figure 11 illustrates the sets used in the global–local search experiments (Section 5.4), which do not include the forward order in the initial candidate pool.

F. Detailed results of loss profiling

In this section, we report the full results of the experiments conducted in Section 5.3. Please refer to Section 5.2 and Section 5.3 for the experimental setup and methodology. Tables 11 to 16 present the success rates of loss profiling on the proposed tasks. In these tables, “Length” denotes the target sequence length, and “Permutation” indicates the specific permutation set used in the experiment. “Top- k Acc” indicates the proportion of trials where the optimal forward order is found within the top k ranked candidates. “Med. Rank” represents the median rank of the forward order among the 128 candidates based on the validation loss.

G. Detailed results of global–local pipeline

In this section, we present the detailed experimental results from the global–local pipeline described in Section 5.4. Table 17 details the actual orders discovered by the pipeline for each task and target length. “Depth” indicates the hierarchy level K

Table 8. Representative input–output samples for each task

| Task | Input | Target |
|--------------------|--|---|
| RELU, $L = 50$ | $X = (4, -7, -7, -3, 8, 1, -8, -9, 8, 6, 0, -9, 5, -9, 6, 5, -5, -9, 7, -5, 8, -6, -7, -2, -7, 6, 7, -2, 0, -6, -3, -8, -7, -8, 3, -1, -6, 1, -4, -9, 2, -7, 1, 4, 9, -5, 6, 2, 3, -3)$ | $Y = (4, 0, 0, 0, 8, 9, 1, 0, 8, 14, 14, 5, 10, 1, 7, 12, 7, 0, 7, 2, 10, 4, 0, 0, 0, 6, 13, 11, 11, 5, 2, 0, 0, 0, 3, 2, 0, 1, 0, 0, 2, 0, 1, 5, 14, 9, 15, 17, 20, 17)$ |
| SQUARE, $L = 50$ | $X = (-5, -9, 8, 7, 8, -7, 5, -9, -6, 9, -2, -8, 6, -7, 2, -7, -6, -5, -5, 7, 3, 6, -9, 1, 7, 0, -7, 7, -5, 0, -2, 6, -1, -9, -6, -7, 0, 2, 7, -1, 1, -2, -6, -7, 5, 1, 9, -6, -3, -3)$ | $Y = (-5, 2, 2, 6, -4, -1, -2, 0, 8, 3, 4, -5, -5, 8, 2, 6, 6, -5, 3, -8, 7, 0, -4, 8, 9, -4, -1, 3, 6, 8, 2, -7, 3, 5, -5, 8, -2, -1, 3, 1, -7, 6, 6, 0, -3, 1, -3, -2, 4, -3)$ |
| TRIANGLE, $L = 50$ | $X = (1, 17, 11, 18, 18, 5, 10, 12, 20, 11, 9, 12, 6, 11, 3, 13, 20, 12, 2, 16, 11, 12, 12, 9, 0, 11, 19, 3, 14, 7, 5, 10, 19, 14, 19, 8, 6, 17, 2, 20, 16, 19, 18, 1, 2, 13, 20, 19, 1, 0)$ | $Y = (1, 2, 7, 5, 3, 12, 2, 6, 6, 3, 8, 0, 14, 5, 12, 5, 5, 3, 15, 11, 2, 6, 2, 9, 11, 2, 1, 16, 10, 3, 12, 2, 1, 5, 4, 8, 6, 3, 15, 15, 11, 10, 8, 11, 7, 0, 0, 1, 18, 2)$ |
| MLP, $L = 50$ | $X = (1, 0, 16, 12, 12, 10, 2, 30, 24, 7, 22, 10, 9, 9, 7, 3, 14, 1, 1, 27, 6, 8, 19, 14, 27, 10, 10, 13, 21, 29, 9, 11, 23, 13, 8, 9, 4, 9, 3, 2, 27, 26, 25, 30, 24, 28, 3, 28, 17, 7)$ | $Y = (1, 30, 16, 21, 19, 21, 0, 21, 14, 24, 14, 22, 23, 23, 26, 0, 26, 2, 29, 11, 25, 25, 15, 20, 13, 22, 22, 19, 16, 12, 23, 20, 15, 21, 24, 23, 30, 24, 0, 30, 11, 17, 14, 13, 15, 13, 29, 11, 20, 25)$ |
| SINE, $L = 50$ | $X = (9, 1, 28, 31, 28, 27, 4, 20, 13, 25, 21, 5, 27, 10, 22, 28, 4, 15, 5, 1, 5, 2, 29, 29, 11, 9, 7, 17, 7, 30, 11, 24, 24, 20, 5, 1, 13, 21, 10, 27, 17, 3, 27, 16, 22, 31, 11, 15, 28, 3)$ | $Y = (9, 25, 28, 3, 25, 4, 0, 4, 6, 25, 25, 25, 4, 25, 25, 28, 31, 25, 25, 25, 25, 3, 31, 28, 6, 25, 31, 31, 6, 4, 25, 6, 25, 3, 0, 6, 28, 6, 31, 25, 25, 28, 6, 6, 28, 3, 25, 0, 28, 25)$ |
| CUBIC, $L = 50$ | $X = (12, 10, 18, 15, 15, 7, 6, 5, 8, 18, 13, 3, 12, 11, 0, 18, 18, 13, 3, 5, 12, 1, 14, 16, 6, 12, 16, 8, 1, 10, 12, 11, 2, 4, 11, 11, 5, 4, 5, 4, 18, 4, 11, 5, 0, 0, 13, 11, 6, 1)$ | $Y = (12, 9, 6, 3, 4, 14, 14, 13, 1, 0, 13, 15, 5, 3, 8, 17, 10, 6, 10, 17, 4, 8, 13, 9, 13, 5, 8, 7, 2, 18, 11, 12, 1, 5, 3, 0, 5, 15, 17, 15, 11, 5, 3, 13, 12, 18, 12, 10, 18, 0)$ |
| PROD, $L = 10$ | $a = (0, 0, 2, 0, 3)$ $b = (0, 2, 6, 3, 7)$ | $Y = (1, 1, 3, 5, 3, 5, 0, 0, 0, 0)$ |

reached in the global stage. The orders are listed relative to the forward sequence (i.e., indices starting from 0 represent the forward order). Orders that successfully recovered the forward sequence are highlighted in bold. We also provide the runtime analysis of the exploration and final training phases in Table 18. The table reports the breakdown of the exploration time into global and local stages, as well as the percentage of time spent on model training during exploration.

Table 9. Parameters for oder-sensitive arithmetic tasks

| Task | Modulus (N) | Input Range (x_i) | Other Constants |
|----------|-----------------|-----------------------|--------------------------|
| RELU | N/A | $\{-9, \dots, 9\}$ | — |
| SQUARE | 19 | $\{-9, \dots, 9\}$ | — |
| CUBIC | 19 | $\{0, \dots, 18\}$ | — |
| TRIANGLE | 20 | $\{0, \dots, 19\}$ | Amplitude $N = 20$ |
| SINE | 32 | $\{0, \dots, 31\}$ | $A = 100, P = 10$ |
| MLP | 32 | $\{0, \dots, 31\}$ | $d_{\text{hidden}} = 64$ |

Table 10. Transformer training configuration

| Hyperparameter | Exploration phase (Small) | Final training phase (Large) | Final training phase (PROD) |
|---------------------------------------|---------------------------|------------------------------|-----------------------------|
| Layers (n_{layer}) | 1 ~ 4 | 6 | 12 |
| Attention Heads (n_{head}) | 1 ~ 4 | 8 | 12 |
| Embedding Dim (d_{emb}) | 128 ~ 512 | 512 | 768 |
| FFN Dim (d_{ffn}) | 512 ~ 2048 | 2048 | 3072 |
| Training samples | 10^5 | 10^5 | 10^6 |
| Batch Size | 32 ~ 128 | 128 | 128 |
| Training Epochs | 1 | 10 | 30 |

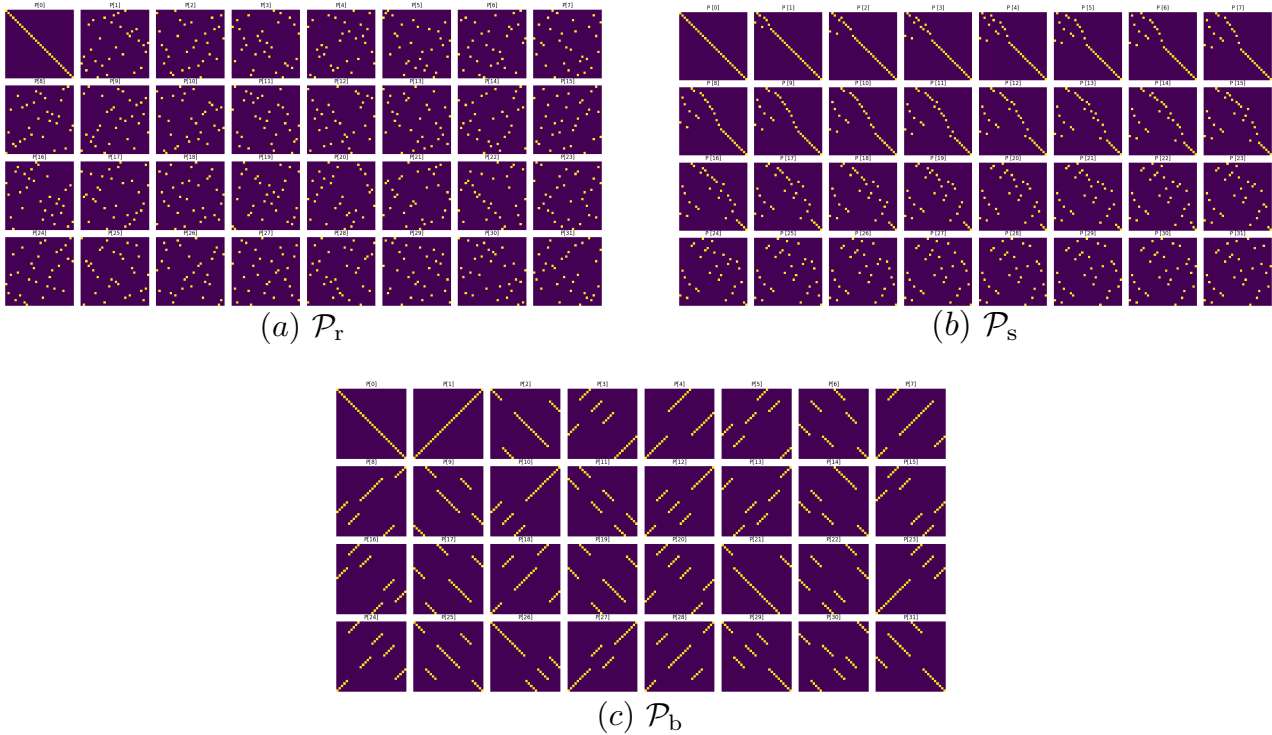


Figure 10. Visualization of the elements in the three permutation sets used in Section 5.3. ID=0 corresponds to the forward (learning-friendly) order.

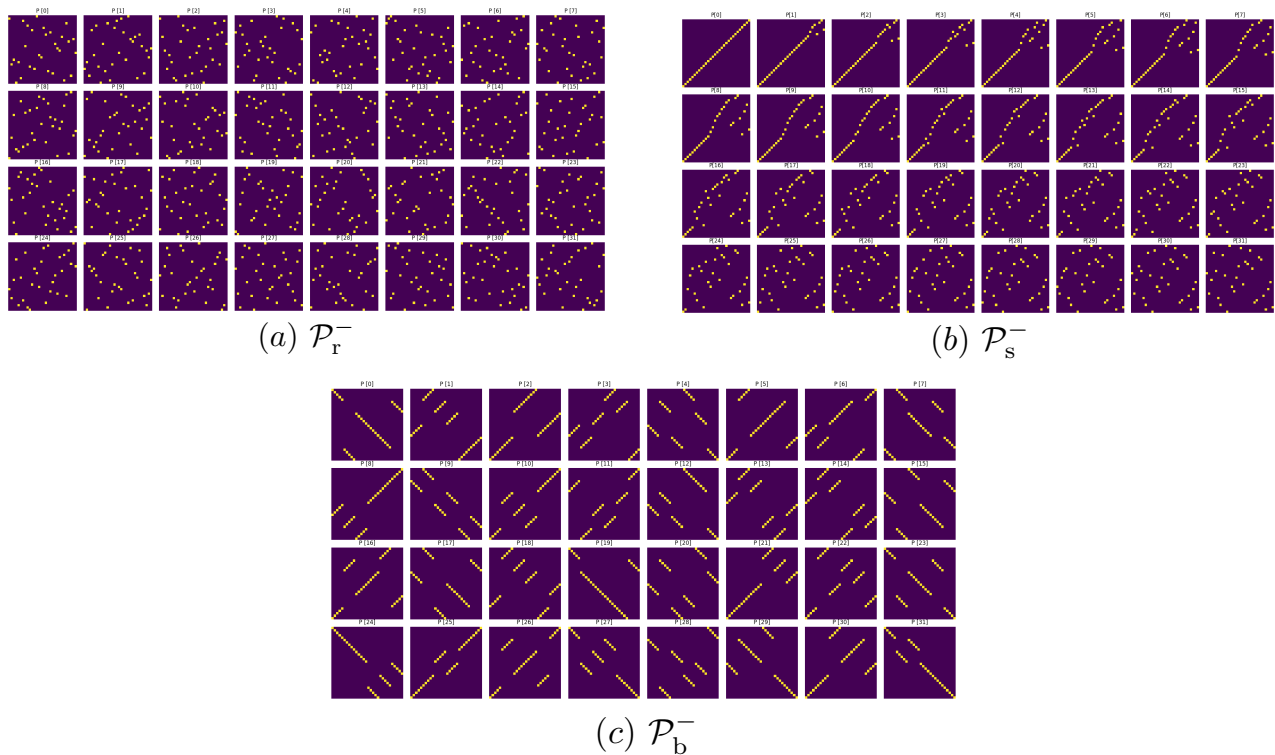


Figure 11. Visualization of the elements in the permutation sets used in Section 5.4. Note that the forward order is not included in the initial candidates.

Table 11. Performance evaluation on RELU task.

| Target Length | Permutation | Top-1 Acc | Top-5 Acc | Top-10 Acc | Med. Rank |
|------------------------------|-----------------|-----------|-----------|------------|-----------|
| $L = 30$ | \mathcal{P}_r | 85.19% | 92.59% | 96.30% | 1.00 |
| | \mathcal{P}_b | 77.78% | 96.30% | 100.00% | 1.00 |
| | \mathcal{P}_s | 96.30% | 100.00% | 100.00% | 1.00 |
| $L = 50$ | \mathcal{P}_r | 100.00% | 100.00% | 100.00% | 1.00 |
| | \mathcal{P}_b | 81.48% | 100.00% | 100.00% | 1.00 |
| | \mathcal{P}_s | 62.96% | 77.78% | 100.00% | 1.00 |
| $L \in \{20, 21 \dots, 30\}$ | \mathcal{P}_r | 62.96% | 81.48% | 88.89% | 1.00 |
| | \mathcal{P}_b | 77.78% | 85.19% | 88.89% | 1.00 |
| | \mathcal{P}_s | 70.37% | 96.30% | 100.00% | 1.00 |
| $L \in \{40, 41 \dots, 50\}$ | \mathcal{P}_r | 96.30% | 100.00% | 100.00% | 1.00 |
| | \mathcal{P}_b | 66.67% | 100.00% | 100.00% | 1.00 |
| | \mathcal{P}_s | 66.67% | 85.19% | 96.30% | 1.00 |

Table 12. Performance evaluation on SQUARE task.

| Target Length | Permutation | Top-1 Acc | Top-5 Acc | Top-10 Acc | Med. Rank |
|------------------------------|-----------------|-----------|-----------|------------|-----------|
| $L = 30$ | \mathcal{P}_r | 77.78% | 85.19% | 85.19% | 4.00 |
| | \mathcal{P}_b | 92.31% | 100.00% | 100.00% | 1.00 |
| | \mathcal{P}_s | 55.56% | 66.67% | 100.00% | 1.00 |
| $L = 50$ | \mathcal{P}_r | 96.30% | 100.00% | 100.00% | 1.00 |
| | \mathcal{P}_b | 62.96% | 66.67% | 66.67% | 1.00 |
| | \mathcal{P}_s | 33.33% | 40.74% | 96.30% | 6.00 |
| $L \in \{20, 21 \dots, 30\}$ | \mathcal{P}_r | 70.37% | 92.59% | 96.30% | 1.00 |
| | \mathcal{P}_b | 96.30% | 100.00% | 100.00% | 1.00 |
| | \mathcal{P}_s | 11.11% | 11.11% | 81.48% | 9.00 |
| $L \in \{40, 41 \dots, 50\}$ | \mathcal{P}_r | 100.00% | 100.00% | 100.00% | 1.00 |
| | \mathcal{P}_b | 66.67% | 66.67% | 66.67% | 1.00 |
| | \mathcal{P}_s | 33.33% | 44.44% | 92.59% | 6.00 |

Table 13. Performance evaluation on SINE task.

| Target Length | Permutation | Top-1 Acc | Top-5 Acc | Top-10 Acc | Med. Rank |
|------------------------------|-----------------|-----------|-----------|------------|-----------|
| $L = 30$ | \mathcal{P}_r | 37.04% | 44.44% | 48.15% | 14.00 |
| | \mathcal{P}_b | 88.89% | 92.59% | 96.30% | 1.00 |
| | \mathcal{P}_s | 11.11% | 66.67% | 70.37% | 3.00 |
| $L = 50$ | \mathcal{P}_r | 55.56% | 77.78% | 77.78% | 1.00 |
| | \mathcal{P}_b | 33.33% | 51.85% | 55.56% | 2.00 |
| | \mathcal{P}_s | 59.26% | 59.26% | 59.26% | 1.00 |
| $L \in \{20, 21 \dots, 30\}$ | \mathcal{P}_r | 18.52% | 25.93% | 44.44% | 11.00 |
| | \mathcal{P}_b | 96.30% | 100.00% | 100.00% | 1.00 |
| | \mathcal{P}_s | 0.00% | 18.52% | 66.67% | 7.00 |
| $L \in \{40, 41 \dots, 50\}$ | \mathcal{P}_r | 62.96% | 66.67% | 77.78% | 1.00 |
| | \mathcal{P}_b | 48.15% | 66.67% | 70.37% | 2.00 |
| | \mathcal{P}_s | 48.15% | 55.56% | 55.56% | 2.00 |

Table 14. Performance evaluation on CUBIC task.

| Target Length | Permutation | Top-1 Acc | Top-5 Acc | Top-10 Acc | Med. Rank |
|------------------------------|-----------------|-----------|-----------|------------|-----------|
| $L = 30$ | \mathcal{P}_r | 18.52% | 22.22% | 22.22% | 83.00 |
| | \mathcal{P}_b | 55.56% | 85.19% | 85.19% | 1.00 |
| | \mathcal{P}_s | 0.00% | 0.00% | 59.26% | 8.00 |
| $L = 50$ | \mathcal{P}_r | 22.22% | 44.44% | 59.26% | 8.00 |
| | \mathcal{P}_b | 55.56% | 66.67% | 66.67% | 1.00 |
| | \mathcal{P}_s | 0.00% | 0.00% | 11.11% | 25.00 |
| $L \in \{20, 21 \dots, 30\}$ | \mathcal{P}_r | 3.70% | 7.41% | 11.11% | 55.00 |
| | \mathcal{P}_b | 74.07% | 100.00% | 100.00% | 1.00 |
| | \mathcal{P}_s | 0.00% | 0.00% | 48.15% | 15.00 |
| $L \in \{40, 41 \dots, 50\}$ | \mathcal{P}_r | 0.00% | 22.22% | 25.93% | 39.00 |
| | \mathcal{P}_b | 74.07% | 77.78% | 77.78% | 1.00 |
| | \mathcal{P}_s | 0.00% | 0.00% | 0.00% | 31.00 |

Table 15. Performance evaluation on MLP task.

| Target Length | Permutation | Top-1 Acc | Top-5 Acc | Top-10 Acc | Med. Rank |
|-------------------------------|-----------------|-----------|-----------|------------|-----------|
| $L = 30$ | \mathcal{P}_r | 22.22% | 25.93% | 37.04% | 26.00 |
| | \mathcal{P}_b | 100.00% | 100.00% | 100.00% | 1.00 |
| | \mathcal{P}_s | 0.00% | 18.52% | 85.19% | 7.00 |
| $L = 50$ | \mathcal{P}_r | 85.19% | 96.30% | 96.30% | 1.00 |
| | \mathcal{P}_b | 88.89% | 100.00% | 100.00% | 1.00 |
| | \mathcal{P}_s | 0.00% | 0.00% | 0.00% | 25.00 |
| $L \in \{20, 21, \dots, 30\}$ | \mathcal{P}_r | 18.52% | 25.93% | 40.74% | 13.00 |
| | \mathcal{P}_b | 100.00% | 100.00% | 100.00% | 1.00 |
| | \mathcal{P}_s | 25.93% | 96.30% | 100.00% | 2.00 |
| $L \in \{40, 41, \dots, 50\}$ | \mathcal{P}_r | 18.52% | 29.63% | 51.85% | 10.00 |
| | \mathcal{P}_b | 66.67% | 85.19% | 88.89% | 1.00 |
| | \mathcal{P}_s | 37.04% | 37.04% | 37.04% | 15.00 |

Table 16. Performance evaluation on TRIANGLE task.

| Target Length | Permutation | Top-1 Acc | Top-5 Acc | Top-10 Acc | Med. Rank |
|-------------------------------|-----------------|-----------|-----------|------------|-----------|
| $L = 30$ | \mathcal{P}_r | 48.15% | 51.85% | 51.85% | 2.00 |
| | \mathcal{P}_b | 96.30% | 100.00% | 100.00% | 1.00 |
| | \mathcal{P}_s | 59.26% | 85.19% | 88.89% | 1.00 |
| $L = 50$ | \mathcal{P}_r | 96.30% | 100.00% | 100.00% | 1.00 |
| | \mathcal{P}_b | 66.67% | 66.67% | 66.67% | 1.00 |
| | \mathcal{P}_s | 37.04% | 37.04% | 37.04% | 12.00 |
| $L \in \{20, 21, \dots, 30\}$ | \mathcal{P}_r | 48.15% | 62.96% | 85.19% | 2.00 |
| | \mathcal{P}_b | 100.00% | 100.00% | 100.00% | 1.00 |
| | \mathcal{P}_s | 7.41% | 59.26% | 85.19% | 4.00 |
| $L \in \{40, 41, \dots, 50\}$ | \mathcal{P}_r | 70.37% | 85.19% | 92.59% | 1.00 |
| | \mathcal{P}_b | 74.07% | 81.48% | 88.89% | 1.00 |
| | \mathcal{P}_s | 33.33% | 33.33% | 37.04% | 13.00 |

Table 17. The orders discovered by the proposed method in its global and local stages. Depth denotes the hierarchy level K reached in the global stage. Each order is listed relative to the forward sequence; when the list starts at 0, the forward order has been recovered. Forward orders identified at a given stage are highlighted in bold.

| Task | Target Length | Depth | Order after global stage | Discovered final order |
|--------|---------------|---------|---|---|
| ReLU | $L = 7$ | $K = 4$ | [6, 0, 5, 2, 3, 4, 1] | [2, 3, 4, 5, 0, 6, 1] |
| | $L = 8$ | $K = 4$ | [0, 2, 1, 3, 4, 5, 6, 7] | [0, 1, 2, 3, 4, 5, 6, 7] |
| | $L = 9$ | $K = 5$ | [0, 1, 2, 3, 4, 5, 6, 7, 8] | [0, 1, 2, 3, 4, 5, 6, 7, 8] |
| | $L = 10$ | $K = 6$ | [6, 7, 8, 9, 5, 4, 2, 3, 1, 0] | [4, 5, 6, 7, 8, 9, 0, 1, 2, 3] |
| | $L = 11$ | $K = 6$ | [8, 9, 10, 7, 6, 5, 4, 3, 2, 1, 0] | [0, 1, 2, 3, 4, 5, 6, 7, 8, 9, 10] |
| | $L = 12$ | $K = 6$ | [6, 7, 8, 9, 10, 11, 5, 4, 2, 3, 1, 0] | [1, 2, 3, 4, 0, 5, 6, 7, 8, 9, 10, 11] |
| | $L = 13$ | $K = 6$ | [11, 12, 10, 9, 8, 7, 6, 5, 4, 2, 3, 1, 0] | [0, 1, 2, 3, 4, 5, 6, 7, 8, 9, 10, 11, 12] |
| SQUARE | $L = 7$ | $K = 4$ | [0, 1, 2, 3, 4, 5, 6] | [0, 1, 2, 3, 4, 5, 6] |
| | $L = 8$ | $K = 4$ | [1, 2, 4, 5, 0, 6, 7, 3] | [1, 2, 4, 5, 0, 6, 7, 3] |
| | $L = 9$ | $K = 5$ | [0, 1, 2, 3, 4, 5, 6, 7, 8] | [0, 1, 2, 3, 4, 5, 6, 7, 8] |
| | $L = 10$ | $K = 6$ | [9, 8, 7, 6, 5, 4, 3, 2, 1, 0] | [0, 1, 2, 3, 4, 5, 6, 7, 8, 9] |
| | $L = 11$ | $K = 6$ | [0, 1, 2, 3, 4, 5, 6, 7, 8, 9, 10] | [0, 1, 2, 3, 4, 5, 6, 7, 8, 9, 10] |
| | $L = 12$ | $K = 6$ | [1, 2, 3, 4, 5, 6, 7, 11, 10, 9, 0, 8] | [0, 1, 2, 3, 4, 5, 6, 7, 8, 9, 10, 11] |
| | $L = 13$ | $K = 6$ | [0, 1, 2, 3, 12, 11, 10, 4, 5, 6, 7, 8, 9] | [8, 9, 0, 1, 2, 3, 4, 10, 11, 12, 5, 6, 7] |
| PROD | $L = 10$ | $K = 6$ | [0, 1, 2, 3, 4, 5, 6, 7, 8, 9] | [0, 1, 2, 3, 4, 5, 6, 7, 8, 9] |

Table 18. Detailed runtime analysis including total exploration time and the proportion of time spent on model training within the exploration phase.

| Search Params | Exploration Time [sec] | | | Training Ratio in Exploration (%) | Final Training [sec] |
|--|------------------------|--------|-------|--------------------------------------|----------------------|
| | Total | Global | Local | | |
| <i>Prod Task</i> | | | | | |
| $K = 6, L = 10$ | 11,729 | 7,001 | 4,448 | 67.6 | 28,213 |
| $K = 6, L = 12$ | 13,436 | 7,301 | 5,935 | 67.9 | 30,695 |
| $K = 7, L = 20$ | 35,981 | 35,981 | — | 11.7 | 38,369 |
| <i>Other (Order-sensitive Synthetic) Tasks</i> | | | | | |
| $K = 6, L = 10$ | 4,424 | 3,912 | 512 | 14.8 | 859 |
| $K = 6, L = 13$ | 4,880 | 4,112 | 768 | 15.1 | 899 |
| $K = 7, L = 20$ | 29,212 | 29,212 | — | 1.7 | 998 |
| $K = 7, L = 30$ | 36,812 | 33,812 | — | 1.7 | 1,206 |
| $K = 7, L = 40$ | 40,351 | 37,351 | — | 1.9 | 1,365 |